Title

Stress Intensity Factor Analysis at an Interfacial Corner between Anisotropic Bimaterials under Thermal Stress

Authors

Yoshiaki Nomura, Toru Ikeda and Noriyuki Miyazaki

Affiliations

Department of Mechanical Engineering and Science, Kyoto University, Yoshida-Honmachi, Sakyo-ku, Kyoto, 606-8501, Japan.

Abstract

A numerical method using a path-independent *H*-integral based on the Betti reciprocal principle was developed to analyze the stress intensity factors of an interfacial corner between anisotropic bimaterials under thermal stress. According to the theory of linear elasticity, asymptotic stress near the tip of a sharp interfacial corner is generally singular as a result of a mismatch of the materials' elastic constants. The eigenvalues and the eigenfunctions are obtained using the Williams

eigenfunction method, which depends on the materials' properties and the geometry of an interfacial corner. The order of the singularity related to the eigenvalue is real, complex or power-logarithmic. The amplitudes of the singular stress terms can be calculated using the *H*-integral. The stress and displacement fields around an interfacial corner for the *H*-integral are obtained using finite element analysis. A proposed definition of the stress intensity factors of an interfacial corner involves a smooth expansion of the stress intensity factors of an interfacial crack between dissimilar materials. The asymptotic solutions of stress and displacement around an interfacial corner are uniquely obtained using these stress intensity factors.

Keywords

H-integral, Stress Singularity, Interfacial Corner, Anisotropic, Thermal Stress, Stress Intensity Factor, Stroh Formalism, Finite Element Method

Main Text

1. Introduction

Micro-structures such as those utilized in electronic devices and micro-electro mechanical systems (MEMS) are composed of many different materials. Many interfacial corners exist in

electronic devices and MEMS because each of the materials employed has a different configuration. Due to a mismatch of the materials' thermal expansion and elastic properties, the stress concentration at an interfacial corner may cause failure. Therefore, the strength of an interfacial corner is very important for the reliability of an electronic product.

Singular stress fields usually occur near the tip of a sharp interfacial corner, and their nature has been the subject of a number of studies. Williams [1] used an eigenvector approach on a corner in homogeneous media, with this method was expanded in a later paper [2]. Stern et al. [3], Sinclair et al. [4], Carpenter [5] and Babuska and Miller [6] employed the Betti reciprocal principle to derive the path-independent *H*-integral and applied this integral to a corner in an isotropic, homogeneous medium for the calculation of stress intensities. This approach was extended to the corner between dissimilar isotropic materials by Carpenter and Byers [7] and Banks-Sills [8], and to the thermal elastic problem by Banks-Sills and Ishbir [9]. Using the Stroh formalism [10] and the *H*-integral, asymptotic solutions to stress and displacement near the corner of dissimilar anisotropic materials have been computed by Labossiere and Dunn [11]. A general solution for the order of the singularity has been provided by Hwu et al. [12], who has also proposed a unified definition for the stress intensity factors of general interfacial corners and cracks [13].

In the present paper, we extend the *H*-integral to analyze asymptotic stress and displacement

fields around an interfacial corner between dissimilar general anisotropic materials under thermal stress, and propose a modified definition of the stress intensity factors of an interfacial corner based on the unified definition proposed by Hwu and Kuo [13]. The *H*-integral is extended to the thermal anisotropic elastic problem using the body force analogy [14]. Employing the Williams eigenfunction expansion method, the Stroh formalism and an extended *H*-integral, asymptotic solutions near an interfacial corner, which are generally mixed-mode, are obtained. The modified definition of stress intensity factors corresponds to the three deformation modes through mode separation from asymptotic stresses. These three stress intensity factors can lead to precise asymptotic solutions of stress and displacement and are directly connected to the stress intensity factors of interfacial cracks proposed by Hwu [15] and those of homogeneous cracks.

2. Singular stress and displacement fields near the tip of an interfacial corner

Consider the wedge corner that consists of *n* different anisotropic elastic materials as shown in Fig. 1. The asymptotic solutions near the tip of a corner under thermal stress have been expressed as follows [9][11]:

$$\begin{aligned} \sigma_{ij}^{k} &= \sum_{m=1}^{\mathrm{N}} C_m r^{\lambda_m - 1} f_{ij}^{mk}(\theta) + \sigma_{ij0}^{k}(\theta) \\ u_i^{k} &= \sum_{m=1}^{\mathrm{N}} C_m r^{\lambda_m} g_i^{mk}(\theta) + u_{i0}^{k}(r,\theta) \end{aligned} \tag{1}$$

where (r,θ) are the polar coordinates whose origin is located on the corner tip, and C_m (m=I,II, … N) is a scalar coefficient obtained by the H-integral, λ_m is the eigenvalue (λ_m-1 is the order of the singularity) and N is the number of eigenvalues. The tensors f_{ij}^{mk} and g_i^{mk} are eigenfunctions related to λ_m which depend upon the angle θ. The last terms of stress and displacement (σ_{ij0}^k, u_{i0}^k) are the regular stress and displacement components, respectively, which are usually absent for mechanical loading [9][16].

The general solutions for eigenvalues and eigenfunctions of general anisotropic multi-bonded materials have been provided by Hwu et al. [12]. By employing the Stroh formalism [10][17], the general solutions near the tip are expressed as

$$\begin{aligned}\mathbf{u}_k &= r^{\lambda}\{\mathbf{A}_k\langle\hat{\mu}_{jk}^{\lambda}(\theta)\rangle\mathbf{c}_k + \overline{\mathbf{A}}_k\langle\overline{\hat{\mu}}_{jk}^{\lambda}(\theta)\rangle\mathbf{d}_k\}\\ \mathbf{t}_k &= \lambda r^{\lambda-1}\{\mathbf{B}_k\langle\hat{\mu}_{jk}^{\lambda}(\theta)\rangle\mathbf{c}_k + \overline{\mathbf{B}}_k\langle\overline{\hat{\mu}}_{jk}^{\lambda}(\theta)\rangle\mathbf{d}_k\}\end{aligned} \tag{2}$$

$$\hat{\mu}_{jk}(\theta) = \cos\theta + \mu_{jk}\sin\theta, \quad j = 1,\ 2,\ 3 \tag{3}$$

where $\mathbf{t}$ is the traction vector related to stresses through $t_i = \sigma_{ij}n_j$ in which n_j denotes the normal vector of the boundary, $\mathbf{A}$ and $\mathbf{B}$ are 3 x 3 complex matrices composed of Stroh's eigenvectors, and μ_j is Stroh's eigenvalue. These eigenvectors and eigenvalues are functions of the anisotropic elastic constants for each material. The vectors $\mathbf{c}_k$ and $\mathbf{d}_k$ are complex coefficient vectors to be determined through the satisfaction of boundary conditions. The angular brackets < > stand for the

3 x 3 diagonal matrix, and the overbar denotes the conjugate of a complex number. Both the1st and *n*th materials have a traction-free boundary condition on their corner flanks, and the tractions and displacements are continuous across each interface at $\theta = \theta_1, \theta_2, ..., \theta_{n-1}$ as shown in Fig. 1. These boundary conditions can be written as

$$\begin{gathered} \mathbf{t}_1(\theta_0) = \mathbf{t}_n(\theta_n) = \mathbf{0} \\ \mathbf{t}_k(\theta_k) = \mathbf{t}_{k+1}(\theta_k),\ \mathbf{u}_k(\theta_k) = \mathbf{u}_{k+1}(\theta_k), \quad k = 1,\ 2,\ ....,\ n-1 \end{gathered} \tag{4}$$

Substituting Eq. (2) into Eq. (4) and using Key matrix $\widehat{\mathbf{N}}$[12], the boundary conditions are simplified as

$$\mathbf{E}_3 \mathbf{p}^* = \mathbf{0}, \qquad \mathbf{E} = \begin{bmatrix} \mathbf{E}_1 & \mathbf{E}_2 \\ \mathbf{E}_3 & \mathbf{E}_4 \end{bmatrix} = \prod_{k=1}^{n} \widehat{\mathbf{N}}_k^{\lambda}(\theta_{k-1}, \theta_k) \tag{5}$$

where

$$\widehat{\mathbf{N}}_k^{\lambda}(\theta_A, \theta_B) = \begin{bmatrix} \mathbf{A}_k & \overline{\mathbf{A}}_k \\ \mathbf{B}_k & \overline{\mathbf{B}}_k \end{bmatrix} \begin{bmatrix} \left\langle \hat{\mu}_{jk}^{\lambda}(\theta_A) \hat{\mu}_{jk}^{-\lambda}(\theta_B) \right\rangle & \mathbf{0} \\ \mathbf{0} & \left\langle \overline{\hat{\mu}}_{jk}^{\lambda}(\theta_A) \overline{\hat{\mu}}_{jk}^{-\lambda}(\theta_B) \right\rangle \end{bmatrix} \begin{bmatrix} \mathbf{B}_k^T & \mathbf{A}_k^T \\ \overline{\mathbf{B}}_k^T & \overline{\mathbf{A}}_k^T \end{bmatrix} \tag{6}$$

Here, $\widehat{\mathbf{N}}$ is a 6 x 6 complex matrix, $\mathbf{E}_3$ is one of the 3 x 3 sub-matrices of the 6 x 6 matrix **E**, and $\mathbf{p}^*$ is a complex vector related to $\mathbf{c}_k$ and $\mathbf{d}_k$. Therefore, the eigenvalue can be obtained by

$$\left\| \mathbf{E}_3 \right\| = 0 \tag{7}$$

In this case, Eq. (7) has an infinite number of possible solutions for λ. Since the displacements are finite, only positive solutions are permitted, i.e., $0 < \mathrm{Re}[\lambda]$, and singular stress terms are dominant near the tip of a corner $\mathrm{Re}[\lambda] < 1$. Thus we will focus only on the region

$$0 < \mathrm{Re}[\lambda] < 1 \tag{8}$$

Using λ_m obtained by Eq. (7) and key matrix $\widehat{\mathbf{N}}$, the eigenfunctions $\mathbf{F}^{mk}$ and $\mathbf{g}^{mk}$ related to f_{ij}^{mk} and g_i^{mk} are expressed as

$$\begin{Bmatrix} \mathbf{g}^{mk}(\theta) \\ \mathbf{F}^{mk}(\theta) \end{Bmatrix} = \begin{cases} \widehat{\mathbf{N}}_k^{\lambda_m}(\theta,\theta_k) \prod_{i=k+1}^{n} \widehat{\mathbf{N}}_i^{\lambda_m}(\theta_{i-1},\theta_i) \begin{Bmatrix} \mathbf{p}^* \\ \mathbf{0} \end{Bmatrix}, & k = 1,\ 2,\ \ldots,n-1 \\ \widehat{\mathbf{N}}_k^{\lambda_m}(\theta,\theta_k) \begin{Bmatrix} \mathbf{p}^* \\ \mathbf{0} \end{Bmatrix}, & k = n \end{cases} \qquad (n > 2) \tag{9}$$

The vector $\mathbf{F}^{mk}$ is the eigenfunction of the stress function $\boldsymbol{\phi}^{mk}$ which is given by

$$\boldsymbol{\phi}^{mk} = C_m r^{\lambda_m} \mathbf{F}^{mk}(\theta) \tag{10}$$

The stress function is related to the stresses by

$$\sigma_{i2} = \phi_{i,1}, \quad \sigma_{i1} = -\phi_{i,2}, \quad i = 1,\ 2,\ 3 \tag{11}$$

From Eqs. (10) and (11), f_{ij}^{mk} is obtained. $\mathbf{g}^{mk}$ and g_i^{mk} have the following relation.

$$\mathbf{g}^{mk}(\theta) = \begin{Bmatrix} g_1^{mk}(\theta) \\ g_2^{mk}(\theta) \\ g_3^{mk}(\theta) \end{Bmatrix} \tag{12}$$

In the singular terms, the only quantities in Eq. (1) that are not obtained are the scalar coefficients C_m which depend on far-field geometry and mechanical and thermal loading.

3. *H*-integral for thermo-elastic problems

We developed a path-independent *H*-integral based on the Betti reciprocal principle in order to

calculate the scalar coefficients C_m subjected to thermo-elastic problems. The Betti reciprocal principle is based on two sets of linear elastic fields: the actual and the complementary. For any closed-contour Γ not containing a singularity, the principle can be written as

$$\oint_{\Gamma}(\sigma_{ij}u_i^* - \sigma_{ij}^* u_i)n_j ds + \int_{\Omega}(s_i u_i^* - s_i^* u_i)d\Omega = 0 \tag{13}$$

where σ_{ij} and u_i are the actual stress and displacement, respectively, σ_{ij}^* and u_i^* are the complementary stress and displacement, respectively, which satisfy the same equilibrium and constitutive relations as the actual fields, s_i and s_i^* are the actual and complementary body forces, respectively, n_j is the unit outward normal to the contour-clockwise Γ, and Ω is the area inside the contour.

Eq. (13) cannot be applied to thermal elastic problems directly. When we consider thermal effects, the Betti reciprocal principle can be rewritten by employing the body force analogy [14] as shown in Fig. 2. According to the analogy, the strain and displacement of a body subjected to thermal elastic forces are identical to those of the same body without thermal loading subjected to the corresponding body forces and tractions. In Fig. 2, ϑ is the change of temperature, s_i and $\tilde{s}_i$ are the body forces, σ_{ij} and $\tilde{\sigma}_{ij}$ are the stresses, and T_i and $\tilde{T}_i$ are the tractions applied to the bodies shown Figs. 2(a) and 2(b), respectively. The body force, stress and traction of the analogous problem ($\tilde{s}_i$, $\tilde{\sigma}_{ij}$, $\tilde{T}_i$) are defined as

$$\begin{aligned}\tilde{s}_i &= s_i - \beta_{ij}\vartheta_{,j} \\ \tilde{\sigma}_{ij} &= \sigma_{ij} + \beta_{ij}\vartheta \\ \tilde{T}_i &= T_i + \beta_{ij}\vartheta n_j\end{aligned} \tag{14}$$

where

$$\beta_{ij} = C_{ijks}\alpha_{ks} \tag{15}.$$

The Betti reciprocal principle for the analogous problem is written as

$$\oint_\Gamma (\tilde{\sigma}_{ij}u_i^* - \tilde{\sigma}_{ij}^* u_i)n_j ds + \int_\Omega (\tilde{s}_i u_i^* - \tilde{s}_i^* u_i)d\Omega = 0 \tag{16}.$$

We consider only that no body forces are present in both the actual and complementary fields. The substitution of Eq. (14) into Eq. (16) and $s_i = s_i^* = 0$ leads to

$$\oint_\Gamma (\sigma_{ij}u_i^* - \sigma_{ij}^* u_i)n_j ds + \oint_\Gamma \beta_{ij}(\vartheta u_i^* - \vartheta^* u_i)n_j ds - \int_\Omega \beta_{ij}(\vartheta_{,j} u_i^* - \vartheta_{,j}^* u_i)d\Omega = 0 \tag{17}.$$

The complementary solutions are chosen as the isothermal problem ($\vartheta^* = 0$). Therefore Eq. (17) becomes

$$\oint_\Gamma (\sigma_{ij}u_i^* - \sigma_{ij}^* u_i)n_j ds + \oint_\Gamma \beta_{ij}\vartheta u_i^* n_j ds - \int_\Omega \beta_{ij}\vartheta_{,j} u_i^* d\Omega = 0 \tag{18}.$$

Applying the Stokes theorem to the second term on the left-hand of Eq. (18), and taking account of the strain-displacement relation, Eq. (18) is written as

$$\oint_\Gamma (\sigma_{ij}u_i^* - \sigma_{ij}^* u_i)n_j ds + \int_\Omega \beta_{ij}\vartheta\varepsilon_{ij}^* d\Omega = 0 \tag{19}.$$

The Betti reciprocal principle for thermo-elastic problems in Eq. (19) is thus obtained. For two-dimensional deformation, the strain-displacement relation becomes

$$\varepsilon_{11}=\frac{\partial u_1}{\partial x_1},\quad 2\varepsilon_{23}=\frac{\partial u_3}{\partial x_2}$$
$$\varepsilon_{22}=\frac{\partial u_2}{\partial x_2},\quad 2\varepsilon_{31}=\frac{\partial u_3}{\partial x_1} \tag{20}$$
$$\varepsilon_{33}=0,\qquad 2\varepsilon_{12}=\frac{\partial u_1}{\partial x_2}+\frac{\partial u_2}{\partial x_1}$$

If this principle is applied to the wedge corner, Γ is selected to be $C_r+C_1+C_2+C_3$ as shown in Fig. 3. The notch flanks are traction-free, and the complementary solutions are taken so that they also satisfy the traction-free condition on the corner flanks. Hence, the line integrals along C_1 and C_3 are zero, and Eq. (19) is written as

$$\int_{C_\delta}(\sigma_{ij}u_i^*-\sigma_{ij}^*u_i)n_j ds=\int_{C_r}(\sigma_{ij}u_i^*-\sigma_{ij}^*u_i)n_j ds+\int_\Omega \beta_{ij}\vartheta\varepsilon_{ij}^* d\Omega \tag{21}$$

where $C_\delta=-C_2$ and a circular contour-clockwise path is selected for the inner path C_δ. The path-independent *H*-integral is defined as the limit of the left-hand term in Eq. (21) for $\delta\to 0$,

$$H=\int_{C_r}(\sigma_{ij}u_i^*-\sigma_{ij}^*u_i)n_j ds+\int_\Omega \beta_{ij}\vartheta\varepsilon_{ij}^* d\Omega \tag{22}$$

where the integral path C_r is arbitrary from the lower flank to the upper flank. The subscript *k* denoting the materials has been neglected for simplicity while the *H*-integral is discussed. Eqs. (13-22) are valid for any multibonded wedges.

4. Interfacial corners between bimaterials

In this section, we consider an interfacial corner between anisotropic bimaterials as shown in Fig.

4, which shows the special case of a wedge corner consisting of *n*-bonded materials (*n*=1 or 2). For an interfacial corner, the combination of the eigenvalues, the calculation of the scalar coefficients by the *H*-integral, the moving least-square method and the definition of the stress intensity factors are treated.

4.1. Five combinations of the eigenvalues

Substituting n = 2, k =*A* or *B* and $\theta_0 = -\beta$, $\theta_1 = 0$, $\theta_2 = \alpha$ into Eqs. (5), (7) and (9), these equations are simplified as

$$\left\|\mathbf{E}_3\right\| = 0, \quad \mathbf{E} = \widehat{\mathbf{N}}_B^{\lambda}(-\beta,0)\widehat{\mathbf{N}}_A^{\lambda}(0,\alpha) \tag{23}$$

$$\begin{Bmatrix} \mathbf{g}^{mk}(\theta) \\ \mathbf{F}^{mk}(\theta) \end{Bmatrix} = \begin{cases} \widehat{\mathbf{N}}_B^{\lambda_m}(\theta,0)\widehat{\mathbf{N}}_A^{\lambda_m}(0,\alpha)\begin{Bmatrix} \mathbf{p}^* \\ \mathbf{0} \end{Bmatrix}, & (-\beta < \theta \le 0) \\ \widehat{\mathbf{N}}_A^{\lambda_m}(\theta,\alpha)\begin{Bmatrix} \mathbf{p}^* \\ \mathbf{0} \end{Bmatrix}, & (0 \le \theta < \alpha) \end{cases} \tag{24}.$$

The λ_m obtained from Eq. (23) in the range of Eq. (8) may be real or complex. If λ_m is a repeated root, the power-logarithmic stress singularities should be considered [18]. Since few situations yield this singular behavior, the power type is not treated in the present study. The combination of λ_m depends upon the wedge angles (α, β) and the anisotropic elastic constants of the two materials, as demonstrated in the following five examples (A-E) [13]:

(A) 3 eigenvalues are real and non-repeated (N=3),

$$0 < \lambda_{\mathrm{I}} < \lambda_{\mathrm{II}} < \lambda_{\mathrm{III}} < 1 \tag{25}$$

(B) 2 eigenvalues are real and non-repeated (N=2),

$$0 < \lambda_{\mathrm{I}} < \lambda_{\mathrm{II}} < 1 \tag{26}$$

(C) 1 eigenvalue is real and is a triple root (N=1),

$$\lambda_{\mathrm{I}} = 0.5 \tag{27}$$

(D) 2 eigenvalues are complex and conjugate, and 1 eigenvalue is real and non-repeated (N=3),

$$\begin{cases} \lambda_{\mathrm{I}} = \lambda + i\varepsilon,\ \lambda_{\mathrm{II}} = \lambda - i\varepsilon,\ \lambda_{\mathrm{III}} = \lambda', & \lambda \le \lambda' \\ \lambda_{\mathrm{I}} = \lambda',\ \lambda_{\mathrm{II}} = \lambda + i\varepsilon,\ \lambda_{\mathrm{III}} = \lambda - i\varepsilon, & \lambda > \lambda' \end{cases} \tag{28}$$

(E) 2 eigenvalues are complex and conjugate (N=2),

$$\lambda_{\mathrm{I}} = \lambda + i\varepsilon,\ \lambda_{\mathrm{II}} = \lambda - i\varepsilon \tag{29}$$

where λ and ε are real numbers. Since the singular terms associated with λ_{I}, λ_{II} and λ_{III} are generally mixed-mode, the subscript has no relation to the three deformation modes. However, when the in-plane and anti-plane deformations can be decoupled, λ_m can be classified into in-plane and anti-plane eigenvalues. Then, regardless of Eqs. (25-29), λ_{III} is chosen to be the anti-plane eigenvalue, which is associated with anti-plane deformation, and the others (λ_{I}, λ_{II}) are the in-plane eigenvalues.

Type (C), which is the case of a homogeneous crack, occurs if we set $\alpha = \beta = \pi$ and two

identical materials $A = B$. In this case, three linearly independent **p*** ($\mathbf{p}_1^*, \mathbf{p}_2^*, \mathbf{p}_3^*$) in Eq. (24) are obtained since λ is a triple root. In spite of N=1, three sets of f_{ij}^{mk} and g_i^{mk} corresponding to $\mathbf{p}_1^*, \mathbf{p}_2^*$, and $\mathbf{p}_3^*$ exist, and three scalar coefficients C_m are needed. In the other cases, the number of C_m which are needed equals N. If λ_m is complex, in the cases of (D) and (E), the corresponding scalar coefficient is also complex, so C_{I} and C_{II} or C_{II} and C_{III} are complex and conjugate.

4.2. Calculation of the scalar coefficients by H-integral

Since the *H*-integral path C_r is arbitrary from the lower flank to the upper flank, a circular contour-clockwise path is selected for simplicity's sake as shown in Fig. 4. If the complementary solutions are chosen properly, *H* equals the scalar coefficient C_m. Szabo and Babuska [19] and Wu and Chang [20] showed that if λ_m is the solution of Eq. (23), $-\lambda_m$ is also the solution. So we chose the complementary solutions as follows.

$$\begin{aligned} \sigma_{ij}^{k*} &= C_m^* r^{-\lambda_m - 1} f_{ij}^{mk*}(\theta) \\ u_i^{k*} &= C_m^* r^{-\lambda_m} g_i^{mk*}(\theta) \end{aligned} \qquad k=A,\ B \tag{30}$$

$$\frac{1}{C_m^*} = \int_{-\beta}^{\alpha} (f_{ij}^{mk}(\theta) g_i^{mk*}(\theta) - f_{ij}^{mk*}(\theta) g_i^{mk}(\theta)) n_j d\theta \tag{31}$$

where f_{ij}^{mk*} and g_i^{mk*} are obtained from Eq. (24) in the same way f_{ij}^{mk} and g_i^{mk} are obtained. These complementary solutions satisfy the requirements mentioned earlier. By shrinking the inner path, the dominant contribution to the solutions inside the region comes from the singular terms. So,

substituting Eqs. (1) and (30) into *H*-integral Eq. (22) in the limit as $\delta \to 0$, and using C^* given in Eq. (31), we obtain

$$H_m = \lim_{\delta \to 0} \int_{-\beta}^{\alpha} (\sigma_{ij}^k u_i^{k*} - \sigma_{ij}^{k*} u_i^k) n_j \delta d\theta = C_m \tag{32}.$$

In the case of m = I, the singular stresses and displacements associated with the minimum eigenvalue λ_{I} of the actual field in Eq. (1) are of the order $O(\delta^{\lambda_{\mathrm{I}}-1})$ and $O(\delta^{\lambda_{\mathrm{I}}})$, respectively. Those of the complementary field in Eq. (30) are of the order $O(\delta^{-\lambda_{\mathrm{I}}-1})$ and $O(\delta^{-\lambda_{\mathrm{I}}})$. Therefore, the products of the above stresses and displacements expressed in Eq. (32) are of the order $O(\delta^{-1})$, and the other terms, whose orders are $O(\delta^{\lambda_{\mathrm{II}}-\lambda_{\mathrm{I}}})$ or $O(\delta^{\lambda_{\mathrm{III}}-\lambda_{\mathrm{I}}})$, are eliminated by $\delta \to 0$. Therefore, only the scalar coefficient C_{I} is left. In the other cases m = II or III, in the same way, the products of the stresses and displacements associated with the eigenvalue λ_{II}, *e.g.* in Eq. (1), and those of the complementary are of the order $O(\delta^{-1})$, but the other terms whose order is $O(\delta^{\lambda_{\mathrm{I}}-\lambda_{\mathrm{II}}})$ cannot be eliminated by $\delta \to 0$. These terms are dissolved by the following relation:

$$\int_{-\beta}^{\alpha} (f_{ij}^{lk}(\theta) g_i^{mk*}(\theta) - f_{ij}^{mk*}(\theta) g_i^{lk}(\theta)) n_j d\theta = 0, \ \ l \neq m \tag{33}.$$

Since the explicit expressions of f_{ij}^{mk}, g_i^{mk}, f_{ij}^{mk*} and g_i^{mk*} are quite complicated, a rigorous proof is not easily performed. Instead, a numerical check has been done for all cases (A-E). Therefore, only C_{II} is left. In order to obtain all the scalar coefficients C_m, we need to evaluate the *H*-integral N times using the N patterns (m = I, II or III)of Eqs. (30) and (31).

On the right-hand side of Eq. (22), the numerical solutions obtained using the finite element method are employed for actual stress and displacement, and Eqs. (30) and (31) are used for the complementary field. Since the strain of the complementary field on the right-hand side of Eq. (22) is of the order $O(r^{-\lambda_m-1})$, the second term is highly singular and cannot be integrated by standard numerical methods near the tip. To overcome this difficulty, the analytic integration is carried out for a radial direction. The complementary strains are expressed as

$$\varepsilon_{ij}^{k*} = C_m^* r^{-\lambda_m-1} h_{ij}^{mk*}(\theta) \tag{34}$$

Using the strain-displacement relation of Eq. (20), h_{ij}^{mk*} is written as

$$\begin{aligned}
h_{11}^{mk*}(\theta) &= -\lambda_m \cos\theta g_1^{mk*}(\theta) - \sin\theta\{g_1^{mk*}(\theta)\}_{,\theta} \\
h_{22}^{mk*}(\theta) &= -\lambda_m \sin\theta g_2^{mk*}(\theta) + \cos\theta\{g_2^{mk*}(\theta)\}_{,\theta} \\
2h_{23}^{mk*}(\theta) &= -\lambda_m \sin\theta g_3^{mk*}(\theta) + \cos\theta\{g_3^{mk*}(\theta)\}_{,\theta} \\
2h_{31}^{mk*}(\theta) &= -\lambda_m \cos\theta g_3^{mk*}(\theta) - \sin\theta\{g_3^{mk*}(\theta)\}_{,\theta} \\
2h_{12}^{mk*}(\theta) &= -\lambda_m \cos\theta g_2^{mk*}(\theta) - \sin\theta\{g_2^{mk*}(\theta)\}_{,\theta} - \lambda_m \sin\theta g_1^{mk*}(\theta) + \cos\theta\{g_1^{mk*}(\theta)\}_{,\theta}
\end{aligned} \tag{35}$$

When the integral path is circular, the element within the region is $rdrd\theta$ [9], and the region is divided into the differential elements of area as shown in Fig. 5. If we assume that the temperature and h_{ij}^{mk*} at the evaluation point are constant in each element, the second term of Eq. (22) can be rewritten as

$$\int_\Omega \beta_{ij}\vartheta\varepsilon_{ij}^{m*} r dr d\theta = \sum_a \sum_b \frac{r_a^{1-\lambda_m} - r_{a-1}^{1-\lambda_m}}{1-\lambda_m} C^* \beta_{ij}\vartheta h_{ij}^{m*}(\theta_b - \theta_{b-1}) \tag{36}$$

where the subscript *k* has been neglected for the sake of simplicity.

4.3. Moving least-square method

The moving least-square method [21] is used as a pre-processing step of the *H*-integral. In many cases, data preparation for post-processing is troublesome. Therefore, using the moving least-square method, the stress, strain and displacement used for the *H*-integral are approximated automatically based on the nodal displacements obtained using the finite element method. The formulation of the moving least-square method is described as follows.

The approximation of displacement at an arbitrary point can be written as

$$\mathbf{u}^h(\boldsymbol{x}) = \mathbf{p}^T(\boldsymbol{x})\mathbf{a}(\boldsymbol{x}) \tag{37}$$

$$\mathbf{p}(\boldsymbol{x}) = \{1, x, y\}^T \tag{38}$$

$\mathbf{a}(\boldsymbol{x})$ is determined by minimizing the following weighted least-square form,

$$\mathbf{R}(\boldsymbol{x}) = \sum_I^n w(\boldsymbol{x} - \boldsymbol{x}_I)[\mathbf{p}^T(\boldsymbol{x}_I)\mathbf{a}(\boldsymbol{x}) - \mathbf{u}_I]^2 \tag{39}$$

where $\mathbf{u}_I$ is the displacement at node I as shown in Fig. 6. The following exponential weight function was employed in this paper.

$$w(d_I) = \begin{cases} \dfrac{\exp(-(d_I/c)^2) - \exp(-(d_{mI}/c)^2)}{1 - \exp(-(d_{mI}/c)^2)}, & \text{if } d_I \le d_{mI} \\ 0, & \text{if } d_I > d_{mI} \end{cases} \tag{40}$$

where $d_I = \|\boldsymbol{x} - \boldsymbol{x}_I\|$, $c = \beta d_{mI}$ and β is a parameter which determines the sharpness of the weight

function. The function $\mathbf{a}(\boldsymbol{x})$ is determined by taking the extremum of $\mathbf{R}(\boldsymbol{x})$ and by substituting $\mathbf{a}(\boldsymbol{x})$ into Eq. (37) to obtain

$$\mathbf{u}^h = \sum_I^n \sum_j^m p_j(\boldsymbol{x})[\mathbf{X}^{-1}(\boldsymbol{x})\mathbf{Y}(\boldsymbol{x})]_{jI}\mathbf{u}_I \equiv \sum_I^n \phi_I(\boldsymbol{x})\mathbf{u}_I \tag{41}$$

where the shape function is given by

$$\phi_I(\boldsymbol{x}) = \sum_j^m p_j(\boldsymbol{x})[\mathbf{X}^{-1}(\boldsymbol{x})\mathbf{Y}(\boldsymbol{x})]_{jI} \tag{42}$$

$$\begin{aligned} \mathbf{X}(\boldsymbol{x}) &= \sum_I^n w(\boldsymbol{x}-\boldsymbol{x}_I)\mathbf{p}(\boldsymbol{x}_I)\mathbf{p}^T(\boldsymbol{x}_I) \\ \mathbf{Y}(\boldsymbol{x}) &= [w(\boldsymbol{x}-\boldsymbol{x}_1)\mathbf{p}(\boldsymbol{x}_1),\ w(\boldsymbol{x}-\boldsymbol{x}_2)\mathbf{p}(\boldsymbol{x}_2),\ \ldots w(\boldsymbol{x}-\boldsymbol{x}_I)\mathbf{p}(\boldsymbol{x}_I)] \end{aligned} \tag{43}.$$

4.4. A modified definition of stress intensity factors

A unified definition of the stress intensity factors of an interfacial corner between anisotropic bimaterials has been proposed by Hwu and Kuo [13], and it is applicable to interfacial cracks [15] and homogeneous cracks considering the consistency of the definition and its clear physical meaning:

$$\mathbf{k} = \begin{Bmatrix} K_{\mathrm{II}} \\ K_{\mathrm{I}} \\ K_{\mathrm{III}} \end{Bmatrix} = \lim_{\substack{r\to 0 \\ \theta=0}} \sqrt{2\pi} r^{1-\mathrm{Re}[\lambda_1]} \mathbf{\Lambda}(\theta) \left\langle (r/l_k)^{-i\varepsilon_*} \right\rangle \mathbf{\Lambda}^{-1}(\theta) \begin{Bmatrix} \sigma_{12} \\ \sigma_{22} \\ \sigma_{32} \end{Bmatrix} \tag{44}$$

where l_k is a length parameter which may be chosen arbitrarily. However, since the stress intensity factors for different l_k cannot be compared, the length parameter should be selected as a fixed value. The matrix $\mathbf{\Lambda}$ is composed of $\mathbf{F}$ obtained from Eq. (24), and < > stands for the diagonal matrix.

In Eq. (44), only the smallest critical eigenvalue λ_{I} is considered. When $r \to 0$, *i.e.* near the tip field, the term associated with λ_{I} will dominate the stress behavior. However, in the actual fracture, the terms associated with minor eigenvalues, λ_{II} or λ_{III}, may have considerable influence. There is a difference between the asymptotic stress considering only the dominant term and that considering all the singular terms, even in the vicinity of a corner. If minor eigenvalues are considered in Eq. (44), more stress intensity factors related to λ_{II} or λ_{III} are needed (six or nine values). No matter how many eigenvalues are considered, it may be convenient for engineers to evaluate a singular stress field using only 3 values, K_{I}, K_{II} and K_{III}.

Therefore, we propose a modified definition of the stress intensity factors based on Eq. (44) for engineering applications, as follows:

$$\mathbf{k} = \begin{Bmatrix} K_{\mathrm{II}} \\ K_{\mathrm{I}} \\ K_{\mathrm{III}} \end{Bmatrix} = \lim_{\substack{r \to 0 \\ \theta = 0}} \sqrt{2\pi r}\, l_k^{0.5 - \mathrm{Re}[\lambda_{\mathrm{I}}]} \mathbf{\Lambda}(\theta) \left\langle (r/l_k)^{0.5-\lambda_m} \right\rangle \mathbf{\Lambda}^{-1}(\theta) \begin{Bmatrix} \sigma_{12} \\ \sigma_{22} \\ \sigma_{32} \end{Bmatrix} \tag{45}$$

$$\mathbf{\Lambda}(\theta) = \left[\mathbf{F}^{\mathrm{I}}(\theta) \quad \mathbf{F}^{\mathrm{II}}(\theta) \quad \mathbf{F}^{\mathrm{III}}(\theta) \right] \tag{46}$$

where l_k is a length parameter which may be chosen arbitrarily, and < > stands for the 3 x 3 diagonal matrix, m=I, II, III. If two eigenvalues exist, as in the cases of (B) and (E), the diagonal matrix and $\mathbf{\Lambda}$ are 2 x 2 and 3 x 2 matrices, respectively. These values have the dimension related to the smallest eigenvalue λ_{I}, because the stress intensity factors which have different dimensions

are unified by the dominant dimension. The physical meaning of this definition is not as clear as that of the definition in Eq. (44). However, since the influence of all the singular terms can be reflected in the stress intensity factors, it is convenient for use in fracture evaluation.

Also, asymptotic solutions of stress and displacement near the tip of an interfacial corner are uniquely obtained using these stress intensity factors. For example, the stresses ahead of an interfacial corner are expressed as

$$\begin{Bmatrix} \sigma_{12} \\ \sigma_{22} \\ \sigma_{32} \end{Bmatrix} = \frac{l_k^{\mathrm{Re}[\lambda_1]-1}}{\sqrt{2\pi}} \mathbf{\Lambda}(0) \left\langle (r/l_k)^{\lambda_m - 1} \right\rangle \mathbf{\Lambda}^{-1}(0) \begin{Bmatrix} K_{\mathrm{II}} \\ K_{\mathrm{I}} \\ K_{\mathrm{III}} \end{Bmatrix} + \begin{Bmatrix} \sigma_{120} \\ \sigma_{220} \\ \sigma_{320} \end{Bmatrix} \tag{47}.$$

The last term on the right-hand side is the regular stress caused by thermal loading [9][16]. Substituting the singular stress terms from Eq. (1) into Eq. (45), the relation between the scalar coefficient C_m and these stress intensity factors is obtained:

$$\begin{Bmatrix} K_{\mathrm{II}} \\ K_{\mathrm{I}} \\ K_{\mathrm{III}} \end{Bmatrix} = \sqrt{2\pi} [C_{\mathrm{I}} l_k^{\mathrm{Im}[\lambda_1]} \begin{Bmatrix} f_{12}^{\mathrm{I}}(0) \\ f_{22}^{\mathrm{I}}(0) \\ f_{32}^{\mathrm{I}}(0) \end{Bmatrix} + C_{\mathrm{II}} l_k^{\lambda_{\mathrm{II}} - \mathrm{Re}[\lambda_1]} \begin{Bmatrix} f_{12}^{\mathrm{II}}(0) \\ f_{22}^{\mathrm{II}}(0) \\ f_{32}^{\mathrm{II}}(0) \end{Bmatrix} + C_{\mathrm{III}} l_k^{\lambda_{\mathrm{III}} - \mathrm{Re}[\lambda_1]} \begin{Bmatrix} f_{12}^{\mathrm{III}}(0) \\ f_{22}^{\mathrm{III}}(0) \\ f_{32}^{\mathrm{III}}(0) \end{Bmatrix}] \tag{48}.$$

In the cases of (B) and (E), the third term is absent. If l_k is changed to l_k', the relation of the stress intensity factors in Eq. (45) is written as

$$\mathbf{k}'(l_k') = \mathbf{\Lambda}(0) \left\langle (l_k / l_k')^{\mathrm{Re}[\lambda_1] - \lambda_m} \right\rangle \mathbf{\Lambda}^{-1}(0) \mathbf{k}(l_k) \tag{49}.$$

This definition involves a smooth expansion of the stress intensity factors of an interfacial crack between dissimilar materials defined by Hwu [15], whose eigenvalues are $\lambda_1 = 0.5 + i\varepsilon$,

$\lambda_{\mathrm{II}} = 0.5 - i\varepsilon$ and $\lambda_{\mathrm{III}} = 0.5$. Thus, Eq. (45) becomes

$$\begin{Bmatrix} K_{\mathrm{II}} \\ K_{\mathrm{I}} \\ K_{\mathrm{III}} \end{Bmatrix} = \lim_{\substack{r\to 0 \\ \theta=0}} \sqrt{2\pi r}\,\mathbf{\Lambda}(\theta)\left\langle (r/l_k)^{-i\varepsilon_m} \right\rangle \mathbf{\Lambda}^{-1}(\theta) \begin{Bmatrix} \sigma_{12} \\ \sigma_{22} \\ \sigma_{32} \end{Bmatrix} \tag{50}$$

where $\varepsilon_{\mathrm{I}} = \varepsilon$, $\varepsilon_{\mathrm{II}} = -\varepsilon$, $\varepsilon_{\mathrm{III}} = 0$ are the anisotropic bimaterial constants. The definition of stress intensity factors in Eq. (45) also has a direct connection with that of a homogeneous crack. In the case of a crack (C), the eigenvalue is $\lambda_{\mathrm{I}} = 0.5$. Then, Eq. (37) becomes

$$\begin{Bmatrix} K_{\mathrm{II}} \\ K_{\mathrm{I}} \\ K_{\mathrm{III}} \end{Bmatrix} = \lim_{\substack{r\to 0 \\ \theta=0}} \sqrt{2\pi r} \begin{Bmatrix} \sigma_{12} \\ \sigma_{22} \\ \sigma_{32} \end{Bmatrix} \tag{51}.$$

5. Numerical results

In the first example, we show the variation of the eigenvalues (A) ~ (E) with respect to the wedge angles. In other examples, the accuracy and efficiency of the present method were examined for several interfacial corner or crack problems. Note that for all the examples, elastic analyses were carried out using the finite element method program for the general plain strain condition. Eight-noded isoparametric elements were used. The moving least-square method was used to determine stresses and displacements along circular paths around an interfacial corner. The length parameter l_k was selected to be 10μm.

5.1. The eigenvalues of an interfacial corner

We calculate λ_m for two cases: glass-silicon bimaterial, and aragonite-Gd_2SiO_5 (GSO) bimaterial interfacial corners. The glass-silicon bimaterial interfacial corner is found in an anodic bonding which is commonly used in micro-sensors. The material properties of glass are E = 72.6 GPa, ν =0.2 and α = 2.0 x 10^{-6} (K^{-1}), while the anisotropic material properties of silicon, aragonite and GSO are shown in Table 1. Silicon and aragonite are made by rotating the principal direction of each material with respect to the x_2-axes (see Fig. 4) –45 degrees. After the rotation, the material properties of silicon and aragonite are

$$C_{\mathrm{Si}} = \begin{bmatrix} 194.4 & 63.9 & 35.2 & 0 & 0 & 0 \\ & 165.7 & 63.9 & 0 & 0 & 0 \\ & & 194.4 & 0 & 0 & 0 \\ & & & 79.6 & 0 & 0 \\ & \text{sym.} & & & 50.9 & 0 \\ & & & & & 79.6 \end{bmatrix} \text{[GPa]}, \quad \alpha_{\mathrm{Si}} = \begin{bmatrix} 3.5 & 0 & 0 \\ 0 & 3.5 & 0 \\ 0 & 0 & 3.5 \end{bmatrix} [10^{-6}\mathrm{K}^{-1}] \qquad (52)$$

$$C_{\mathrm{aragonite}} = \begin{bmatrix} 87.8 & 26.3 & 36.6 & 0 & 18.75 & 0 \\ & 87 & 26.3 & 0 & 10.35 & 0 \\ & & 87.8 & 0 & 18.75 & 0 \\ & & & 42 & 0 & 0.7 \\ & \text{sym.} & & & 60.27 & 0 \\ & & & & & 42 \end{bmatrix} \text{[GPa]}, \quad \alpha_{\mathrm{aragonite}} = \begin{bmatrix} 22.5 & 0 & 12.5 \\ 0 & 17 & 0 \\ 12.5 & 0 & 22.5 \end{bmatrix} [10^{-6}\mathrm{K}^{-1}] \quad (53).$$

Consider an interfacial corner between glass-silicon bimaterials. In order to explore the dependence of the eigenvalue on the wedge angle and compare it with Labossiere and Dunn's results [11], we plot $1-\lambda_m$ versus the wedge angle of silicon β in Fig. 7. The wedge angle of

glass, $\alpha = 180°$, is fixed. The results are the same as Labossiere's results, where only in-plane deformations were focused on and the λ_{III} in Fig. 7 related to anti-plane deformations was absent. For $0° < \beta < 69°$, two eigenvalues are real, corresponding to (B) in Section 4.1. For $69° < \beta < 143°$, three eigenvalues are real, corresponding to (A). At $\beta \approx 143°$, the power-logarithmic stress singularity should be considered, because λ_I and λ_{II} have the same value, which is a repeated root. For $143° < \beta < 180°$, two eigenvalues are a complex conjugate whose real number is a repeated root, and the other is a real eigenvalue, corresponding to (D). $\beta = 180°$ is a well known case of an interfacial crack.

Consider an interfacial corner between aragonite-GSO bimaterials. A plot of $1 - \lambda_m$ versus the wedge angle of GSO β' is shown in Fig. 8, and that of aragonite $\alpha = 90°$ is fixed. For $90° < \beta' < 127°$, two eigenvalues are complex and conjugate corresponding to (E). The power-logarithmic stress singularity should be considered at $\beta' \approx 127°$. For $127° < \beta' < 173°$, two real eigenvalues exist corresponding to (B). For $173° < \beta' \leq 180°$, three real eigenvalues exist corresponding to (A). Since (C) is the case of a crack in a homogeneous body, (C) is absent in these two examples.

5.2. Stress intensity factors of interfacial corners under thermal stress

We consider an interfacial corner configuration as shown in Fig. 9. The wedge angles of glass and silicon are $\alpha = 180°$ and $\beta = 125.26°$, respectively. The stress intensity factors in Eq. (45) subjected to a uniform change of temperature $\vartheta = +100\text{K}$ and a uniform tension $\sigma = 0.1\text{MPa}$ applied at the edge of glass were analyzed. The material properties of glass and silicon are the same as in Section 5.1. The numbers of nodes and elements of the FE mesh, whose smallest element near the tip was 0.0001 mm, were 8,583 and 2,782, respectively.

The eigenvalues were $\lambda_{\text{I}} = 0.5033$, $\lambda_{\text{II}} = 0.6368$ and $\lambda_{\text{III}} = 0.5485$. Six different radii r of the H-integral path were examined. Stress intensity factors whose dimensions were related to the smallest eigenvalue λ_{I} are shown in Table 2. They are stable and path-independent for values of r larger than 0.001 mm. By substituting the stress intensity factors obtained by the H-integral, whose path r = 0.01 mm, into Eq. (47), the stress distribution ahead of an interfacial corner was calculated, where the regular terms were ignored. Excellent agreement between those results and the finite element solutions is shown in Fig. 10, and the accuracy of the stress intensity factors was indirectly demonstrated.

For the purpose of comparison, two asymptotic stress distributions ahead of an interfacial corner are shown in Fig. 11. One is the summation of the singular terms associated with λ_{I} and λ_{II}, and the other is only the dominant singular term with λ_{I}. They should correspond to each other as the

limit for $r \to 0$, but there is great difference even at 10^{-8}mm in Fig. 11. Therefore, the influence of minor eigenvalues should be considered for the actual fracture, and we thus modified the definition of stress intensity factors in Eq. (44).

In this case, the in-plane and anti-plane deformations are decoupled, since both silicon and glass possess a material symmetrical plane identical to the coordinate plane $x_3 = 0$. Thus, the contribution of the singular term with λ_{III} related to anti-plane deformations was zero, and the stress intensity factor of the tearing mode K_{III} was almost negligible.

An interfacial corner subjected to a uniform change of temperature $\vartheta = -20\mathrm{K}$ as shown in Fig. 12 was analyzed. The wedge angles of aragonite and GSO are $\alpha = 180°$ and $\beta = 160°$, respectively. The material properties of aragonite were given in Eq. (53) and those of GSO as shown in Table 1 were used. The numbers of nodes and elements of the FE mesh were 8,431 and 2,734, respectively.

The eigenvalues, scalar coefficients, and stress intensity factors are shown in Table 3. The scalar coefficients C_m and the stress intensity factors K have the relation given in Eq. (48). The stress distribution obtained from Eq. (47) and the finite element solutions ahead of an interfacial corner are shown in Fig. 13, where close agreement between those results can be seen. This fact indirectly

proved the reasonableness of the analyzed stress intensity factors as well. In Table 3, K_{III} is relatively large because the in-plane and anti-plane deformations are coupled in the case of orthotropic and monoclinic bimaterial corners. The eigenvalues, eigenfunctions and scalar coefficients of the first and second terms (I and II) were complex and conjugate. The three scalar coefficients had no relation to the three deformation modes, opening, sliding and tearing, as shown by the stress distribution in Fig. 13. Therefore, the scalar coefficients are inappropriate as a criterion for an interfacial corner. On the other hand, the ratio of the stress intensity factors that were proposed in this study corresponds to the proportion of stress in the three deformation modes qualitatively, and thus these stress intensity factors were easily understandable.

A single-edge interfacial crack between aragonite-GSO bimaterials subjected to a non-uniform change of temperature was examined as illustrated in Fig. 14. The change of temperature has a uniform gradient with respect to the x_1-direction, –100/3 [K/mm]. The interfacial crack is a special case of an interfacial corner with wedge angles $\alpha = \beta = 180°$. The material properties of aragonite and GSO are also those given in Table 1, while the numbers of nodes and elements of the FE mesh were 10,547 and 3,436, respectively.

The eigenvalues were $\lambda_{I} = 0.5 + 0.0292i$, $\lambda_{II} = 0.5 - 0.0292i$ and $\lambda_{III} = 0.5$, where 0.0292 was

the bimaterial constant. For the purpose of comparison, we evaluated the stress intensity factors defined in Eq. (45) through the use of both the present method and the *M*-integral method [22]. The stress intensity factors obtained by these two methods versus *r/m* are shown in Fig. 15, where *r* and *m* stood for the radius of the *H*-integral circular path and the smallest element size 0.0001 mm, respectively. In the near tip region $r/m < 3\sim 4$, the stress intensity factors were unstable, because the singular point yielded errors in the FEM solutions near the tip which were used to calculate those stress intensity factors. On the other hand, in the outer region $r/m > 3\sim 4$, the stress intensity factors determined by the present method were stable and agreed well with those obtained by the *M*-integral method. Thus, the *H*-integral path should be far from this near-tip region in order to obtain accurate results. Furthermore, the present method could be used to analyze an interfacial crack, and the stress intensity factors of an interfacial corner defined in Eq. (45) involved that of an interfacial crack as defined in Eq. (50).

6. Conclusion

A numerical method using the path-independent *H*-integral based on the Betti reciprocal principle was developed to analyze the stress intensity factors of an interfacial corner between anisotropic bimaterials under thermal stress. To evaluate the amplitudes of the analyzed singular

stress field, a new definition of the stress intensity factors of an interfacial corner, which involved a smooth expansion of the stress intensity factors of an interfacial crack, was proposed. Using these stress intensity factors, asymptotic solutions of stress and displacement around an interfacial corner can be uniquely obtained. Moreover, the deformation mode can be easily understood qualitatively, since the three stress intensity factors correspond to the proportions of the opening, sliding and tearing modes, respectively. Using this numerical method, analyses of interfacial corners subjected to thermal and mechanical loading were performed, and the stress intensity factors were calculated. The asymptotic stress solutions obtained by the stress intensity factors showed excellent agreement with the finite element solutions, thus demonstrating the accuracy of the present method.

References

[1] Williams ML. Stress singularities resulting from various boundary conditions in angular corners of plates in extension. Journal of Applied Mechanics 1952;19:526-528.

[2] Williams ML. On the stress distribution at the base of a stationary crack. Journal of Applied Mechanics 1957;24:109-114.

[3] Stern M, Becker EB, Dunham RS. A contour integral computation of mixed-mode stress intensity factors. International Journal of Fracture 1976;12:359-368.

[4] Sinclair GB, Okajima M, Griffin JH. Path independent integrals for computing stress intensity factors at sharp corners in elastic plates. International Journal for Numerical Methods in Engineering 1984;20:999-1008.

[5] Carpenter WC. Calculation of fracture parameters for a general corner. International Journal of Fracture 1984;24:45-58.

[6] Babuska I, Miller A. The post-processing approach in the finite element method —Part 2: the calculation of stress intensity factors. International Journal for Numerical Methods in Engineering 1984;20:1111-1129.

[7] Carpenter WC, Byers C. A path independent integral for computing stress intensities for V-notched cracks in a bi-material. International Journal of Fracture 1987;35:245-268.

[8] Banks-Sills L. A conservative integral for determining stress intensity factors of a bimaterial strip. International Journal of Fracture 1997;86:385-398.

[9] Banks-Sills L, Ishbir C. A conservative integral for bimaterial notches subjected to thermal stresses. International Journal for Numerical Methods in Engineering 2004;60:1075-1102.

[10] Stroh AN. Dislocations and cracks in anisotropic elasticity. Philosophical Magazine 1958;3:625-626.

[11] Labossiere PEW, Dunn ML. Stress intensities at interface corners in anisotropic bimaterials. Engineering Fracture Mechanics 1999;62:555-575.

[12] Hwu C, Omiya M, Kishimoto K. A key matrix N for the stress singularity of the anisotropic elastic composite wedges. JSME International Journal Series A 2003;46:40-50.

[13] Hwu C, Kuo TL. A unified definition for stress intensity factors of interface corners and cracks. International Journal of Solids and Structures 2007;44:6340-6359.

[14] Boley BA, Weiner JH. Theory of Thermal Stresses. Wiley: New York, 1962.

[15] Hwu C. Explicit solutions for collinear interface crack problems. International Journal of Solids and Structures 1993;30:301-312.

[16] Fränkle M, Munz D, Yang YY. Stress singularities in a bimaterial joint with inhomogeneous temperature distribution, International Journal of Solids and Structures, 1996;33:2039-2054.

[17] Ting TCT. Anisotropic Elasticity: Theory and Application. Oxford University Press 1996.

[18] Dempsey JP. Power-logarithmic stress singularities at bi-material corners and interface cracks. Journal of Adhesion Science and Technology 1995;9:253-265.

[19] Szabo BA, Babuska I. Computation of the amplitude of stress singular terms for cracks and reentrant corners. ASTM, Philadelphia, 1988. STP 969. pp.101-124.

[20] Wu KC, Chang FT. Near-tip fields in a notched body with dislocations and body forces. Journal of Applied Mechanics 1993;60:936-941.

[21] Nyroles B, Touzot G, Villon P. Generalizing the finite element method: diffuse approximation and diffuse elements. Comput Mech 1992;10:307-318.

[22] Nagai M, Ikeda T, Miyazaki N. Stress intensity factor analysis of a three-dimensional interface crack between dissimilar anisotropic materials. Engineering Fracture Mechanics 2007;74:2481-2497.

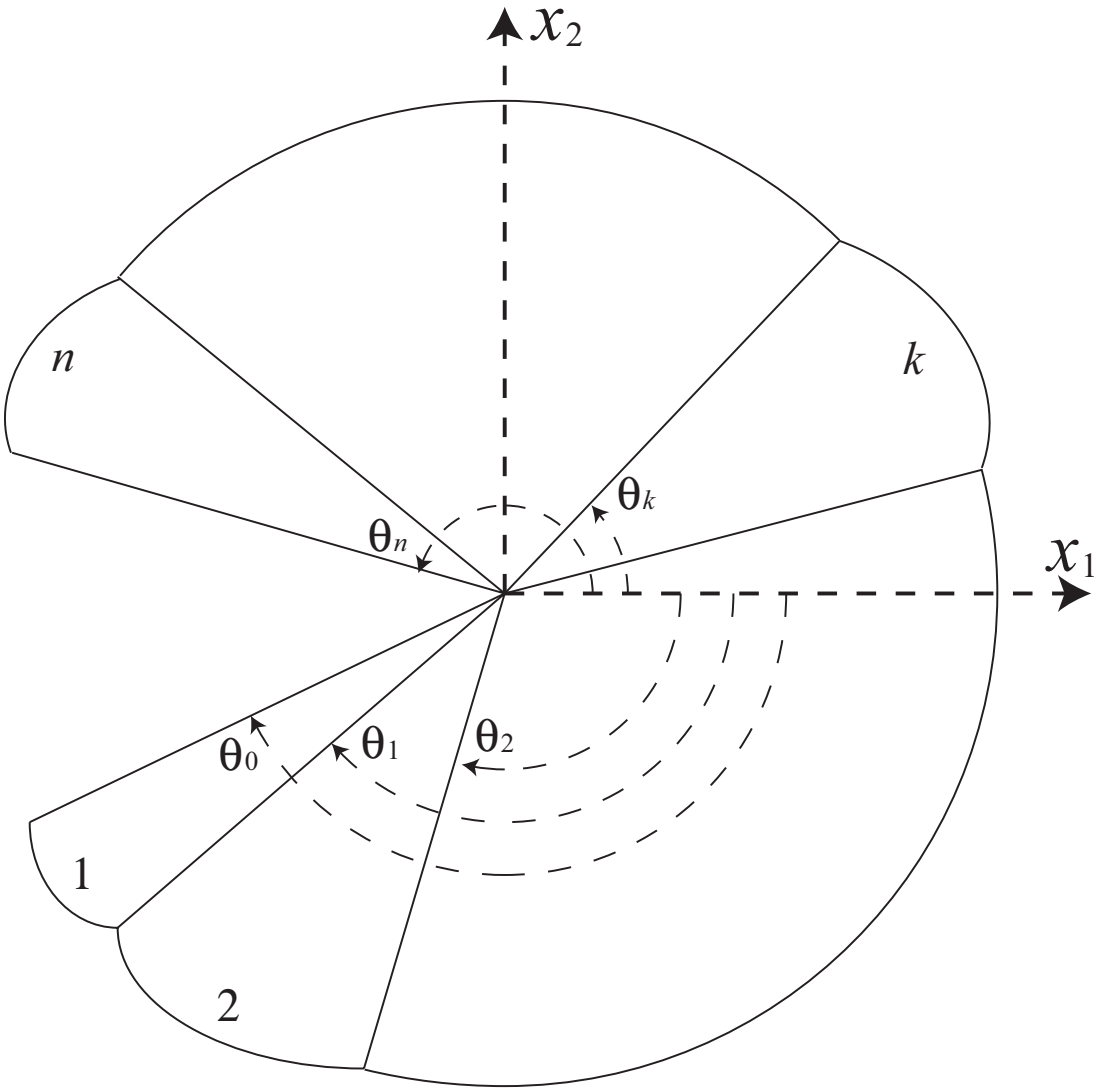

Fig. 1 Geometry of anisotropic n-multibonded materials.

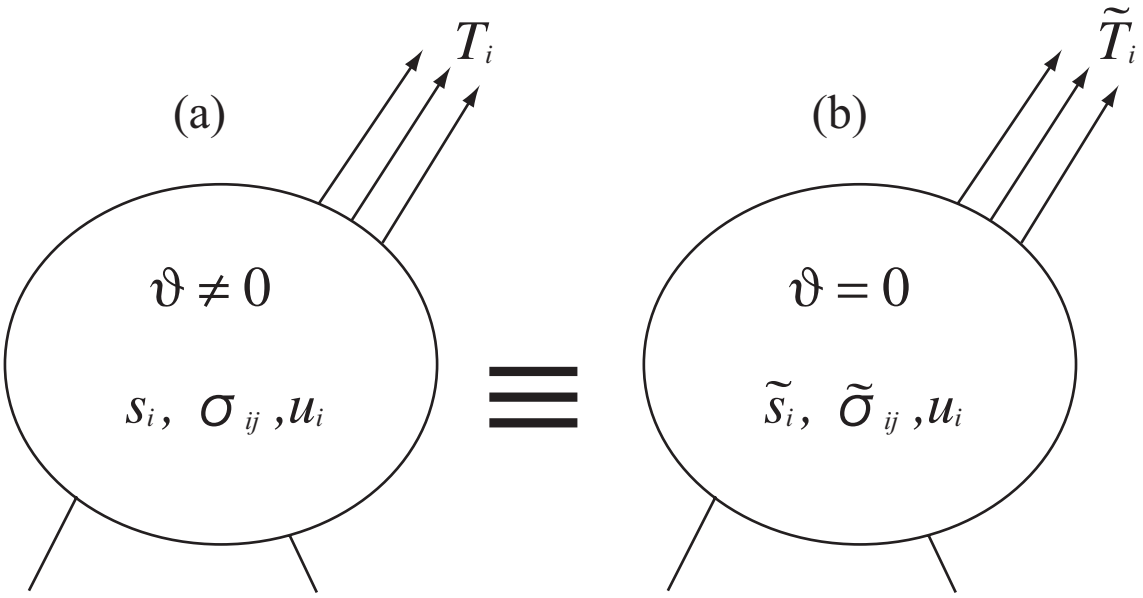

Fig. 2 Body force analogy (a) the original body (b) the analogous body.

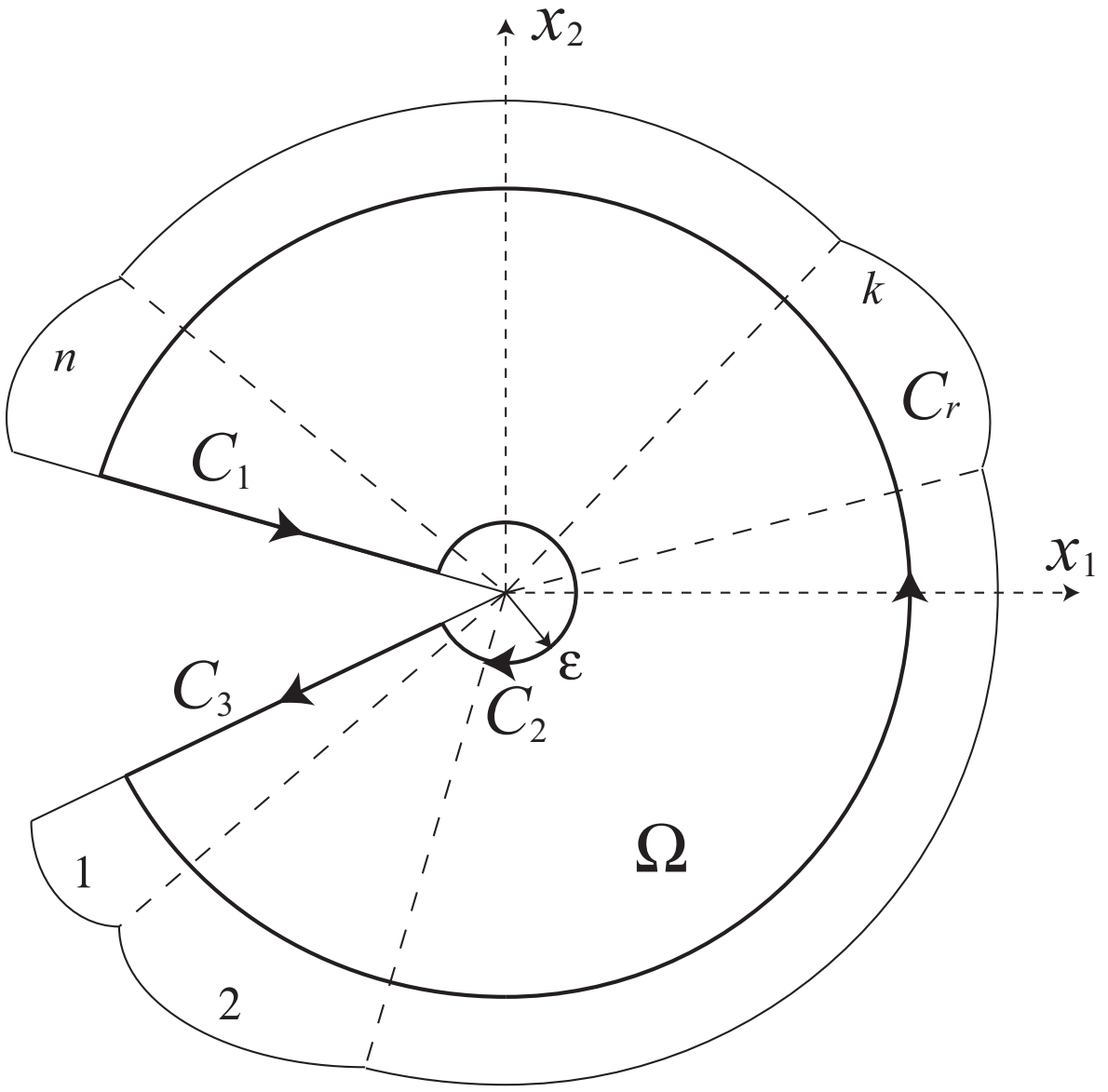

Fig. 3 Schematic of the H-integral contour in a multibonded body.

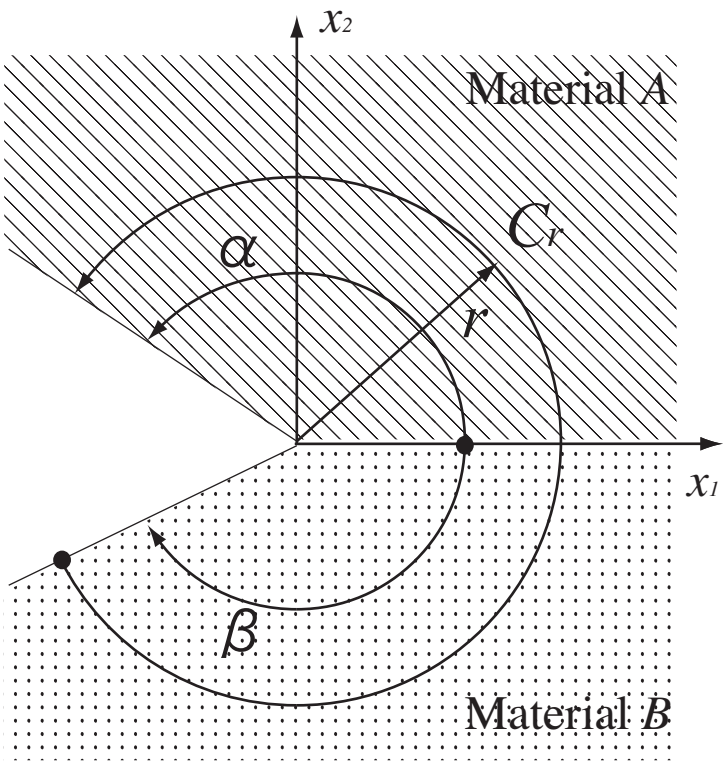

Fig. 4 Geometry of an interfacial corner.

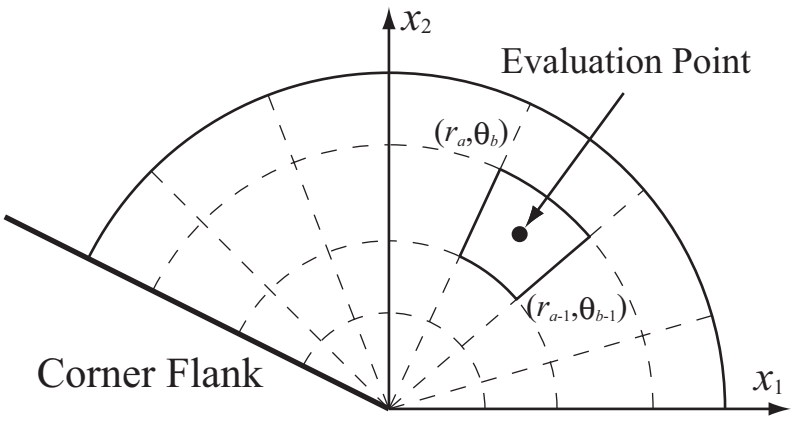

Fig. 5 The divided elements within the surface integral region.

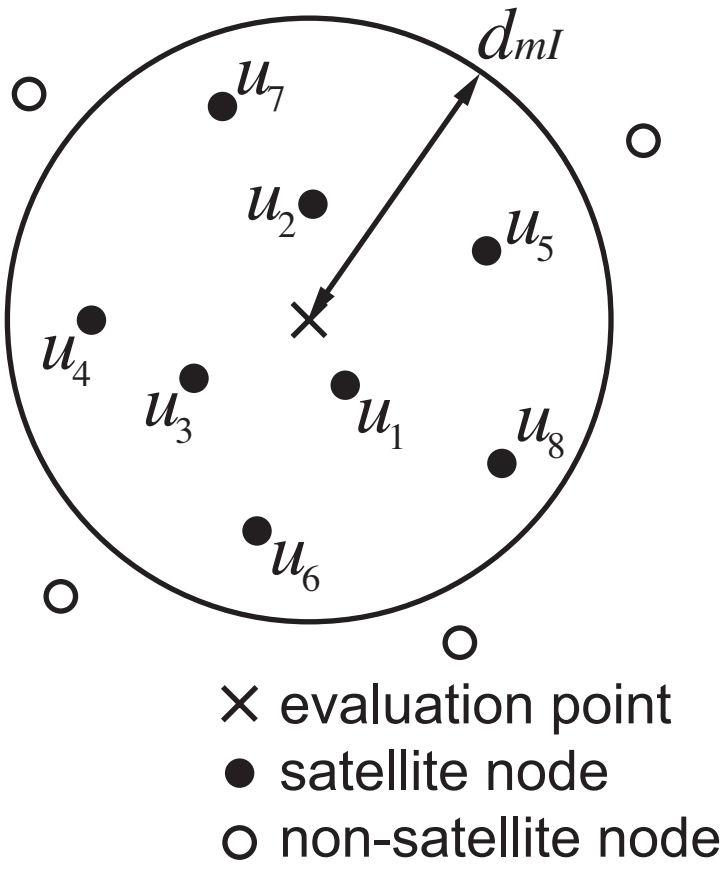

Fig. 6 The concept of the moving least-square method.

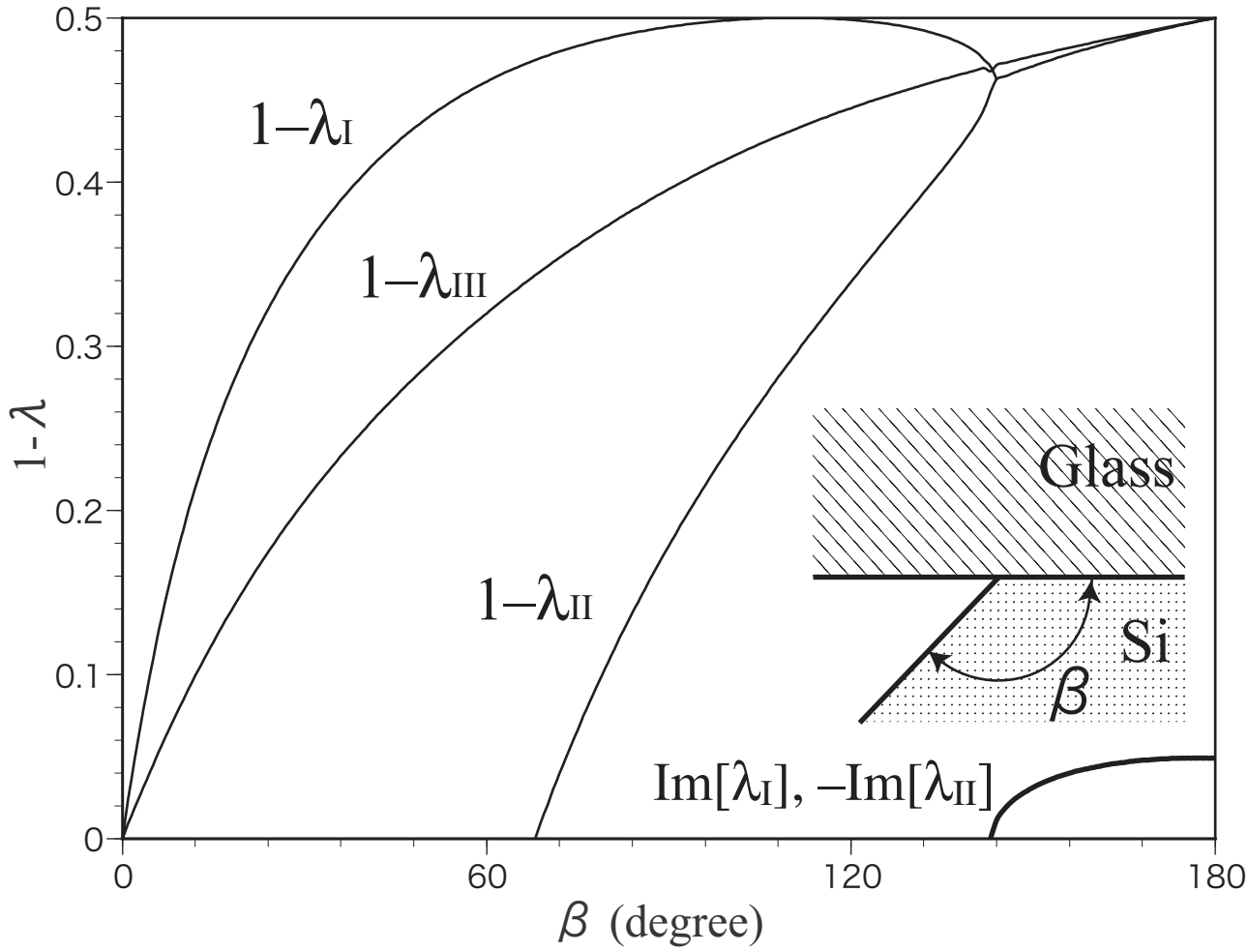

Fig. 7 Singular exponent for an interfacial corner between glass-silicon bimaterials.

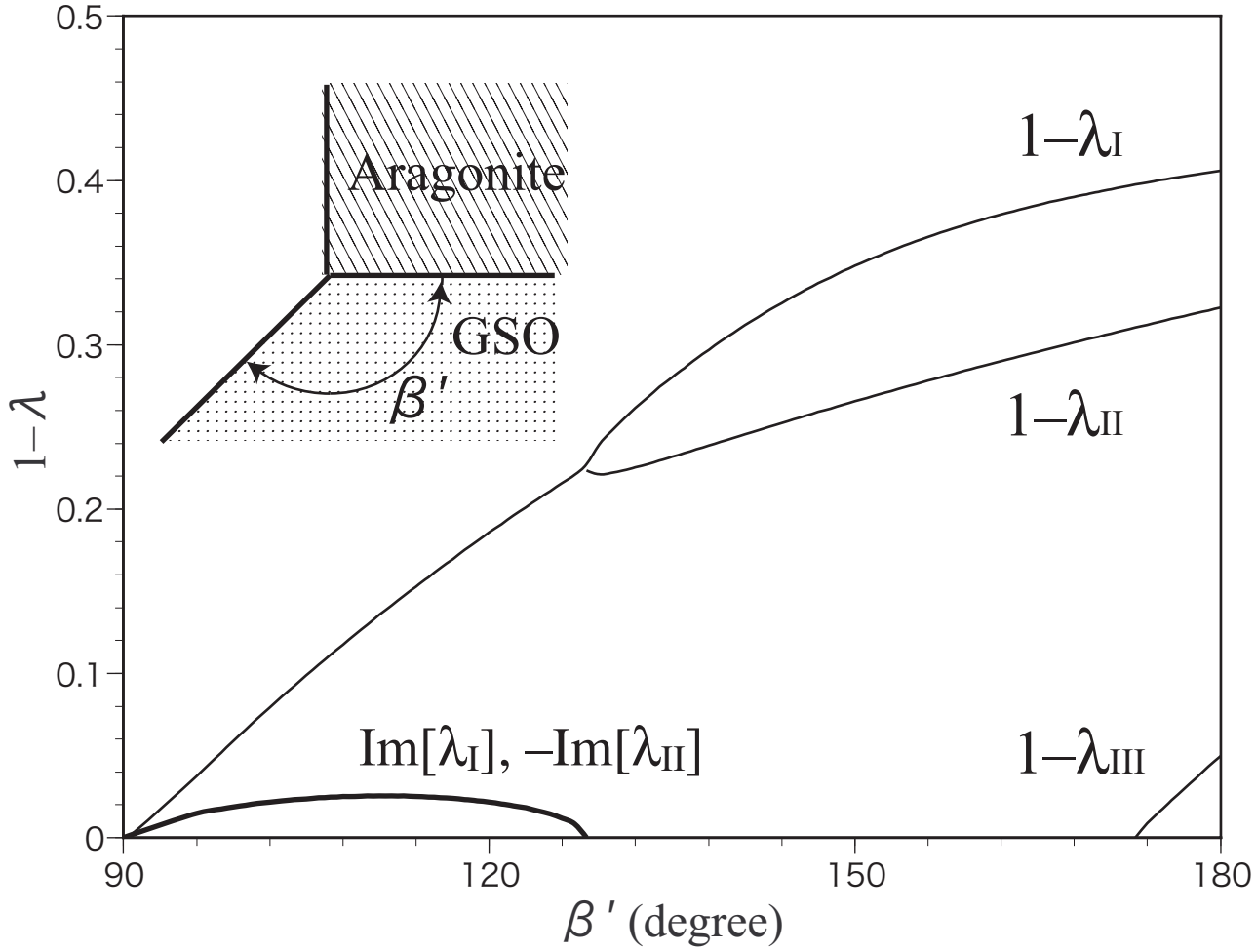

Fig. 8 Singular exponent for an interfacial corner between aragonite-GSO bimaterials.

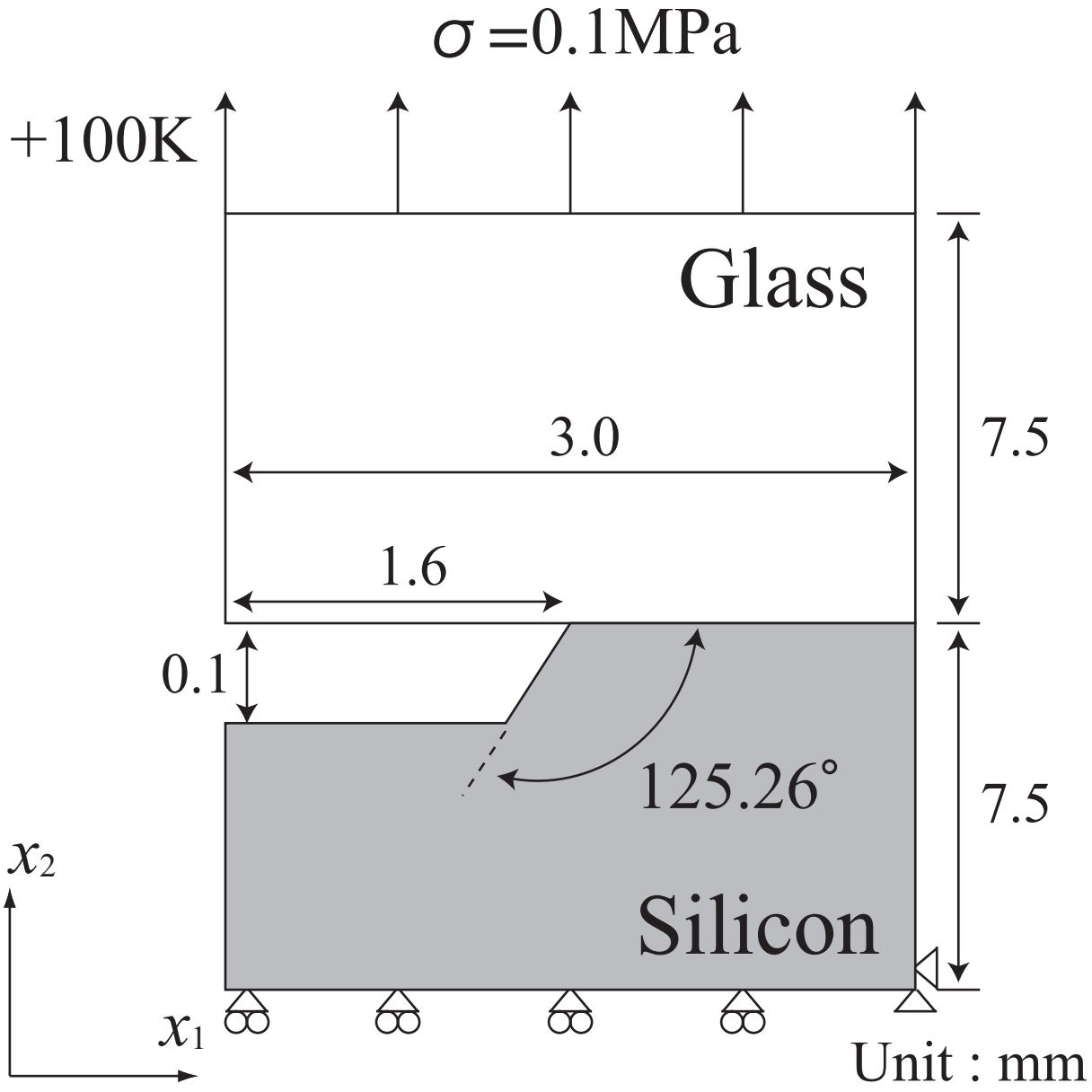

Fig. 9 Interfacial corner between isotropic-anisotropic bimaterials (uniform tension 0.1 MPa and change of temperature +100K).

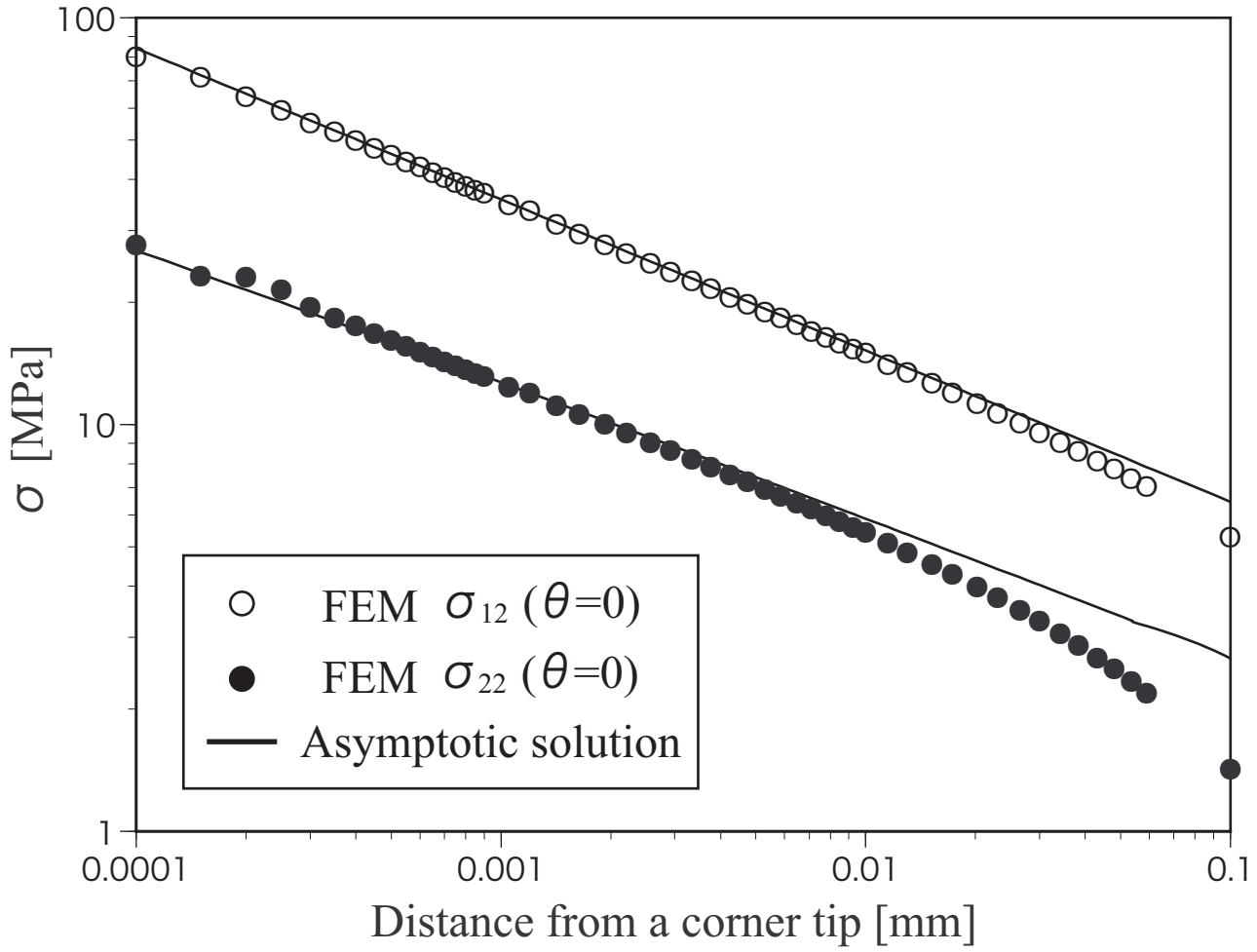

Fig. 10 Stress distribution along a glass-silicon bimaterial interface.

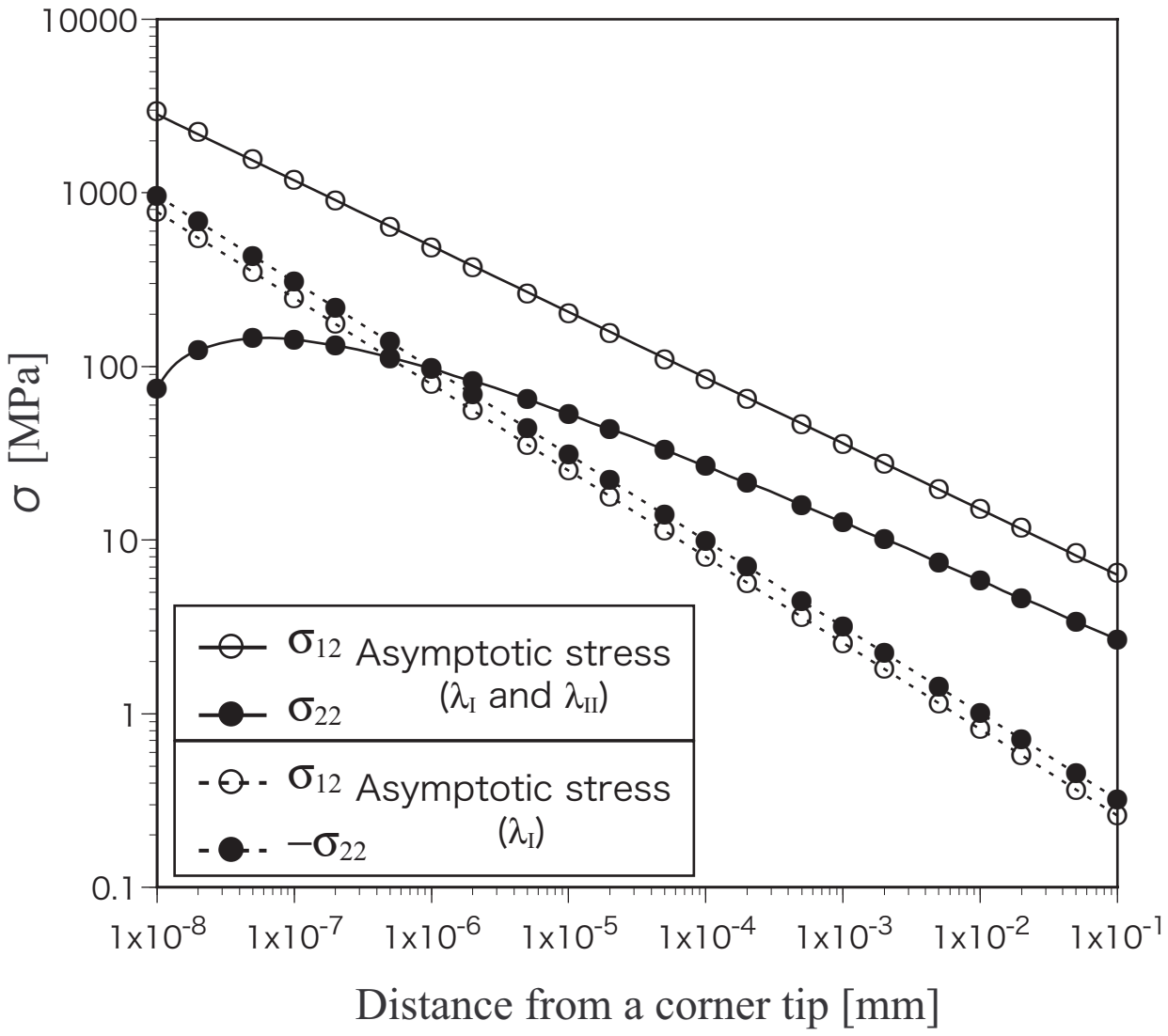

Fig. 11 Asymptotic stress distributions along a glass-silicon interface. (The solid lines are the summation of the terms associated with and ; the dashed lines are the term with only .)

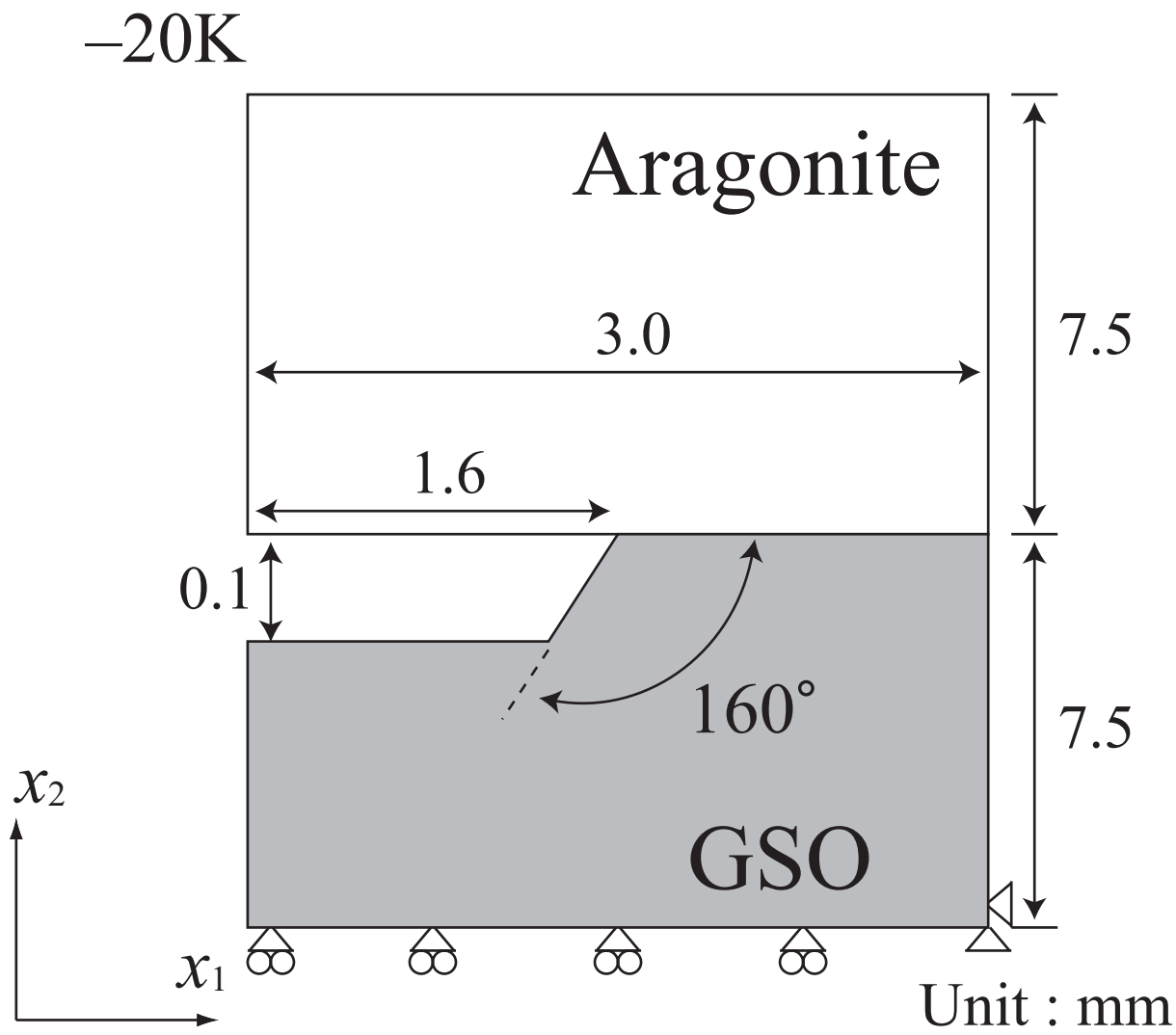

Fig. 12 Interfacial corner between anisotropic bimaterials (uniform change of temperature –20K).

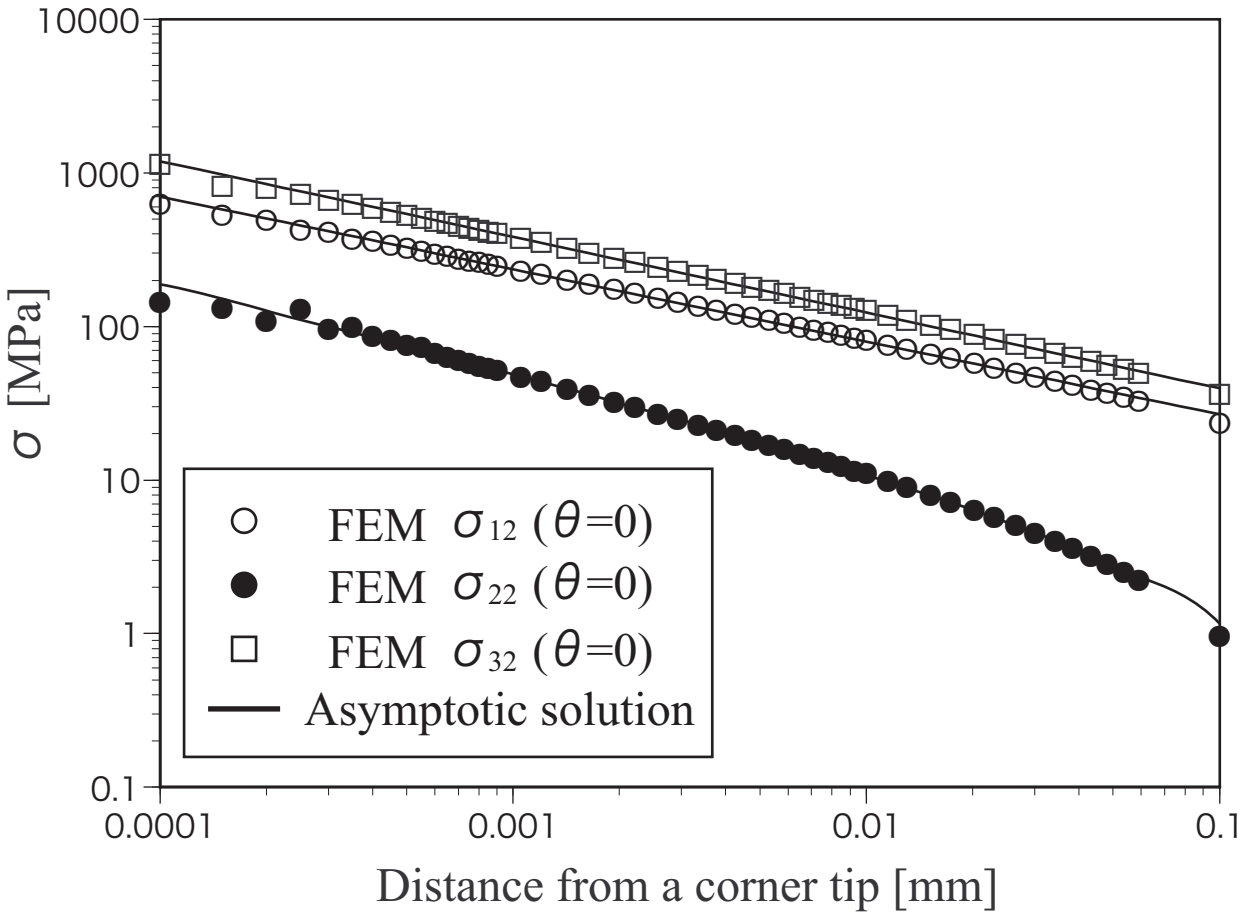

Fig. 13 Stress distribution along an aragonite-GSO bimaterial interface.

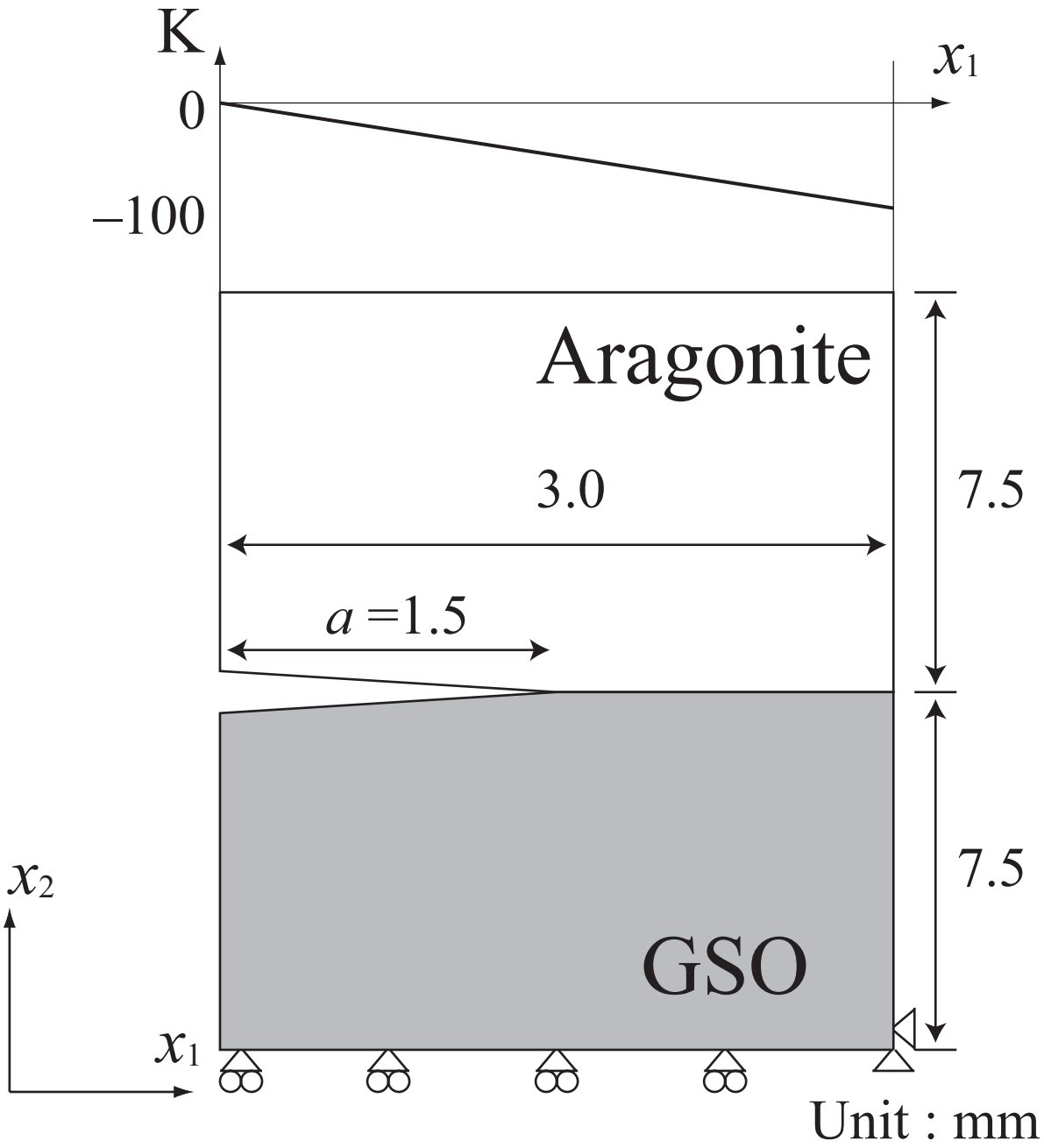

Fig. 14 Interfacial crack between anisotropic bimaterials.

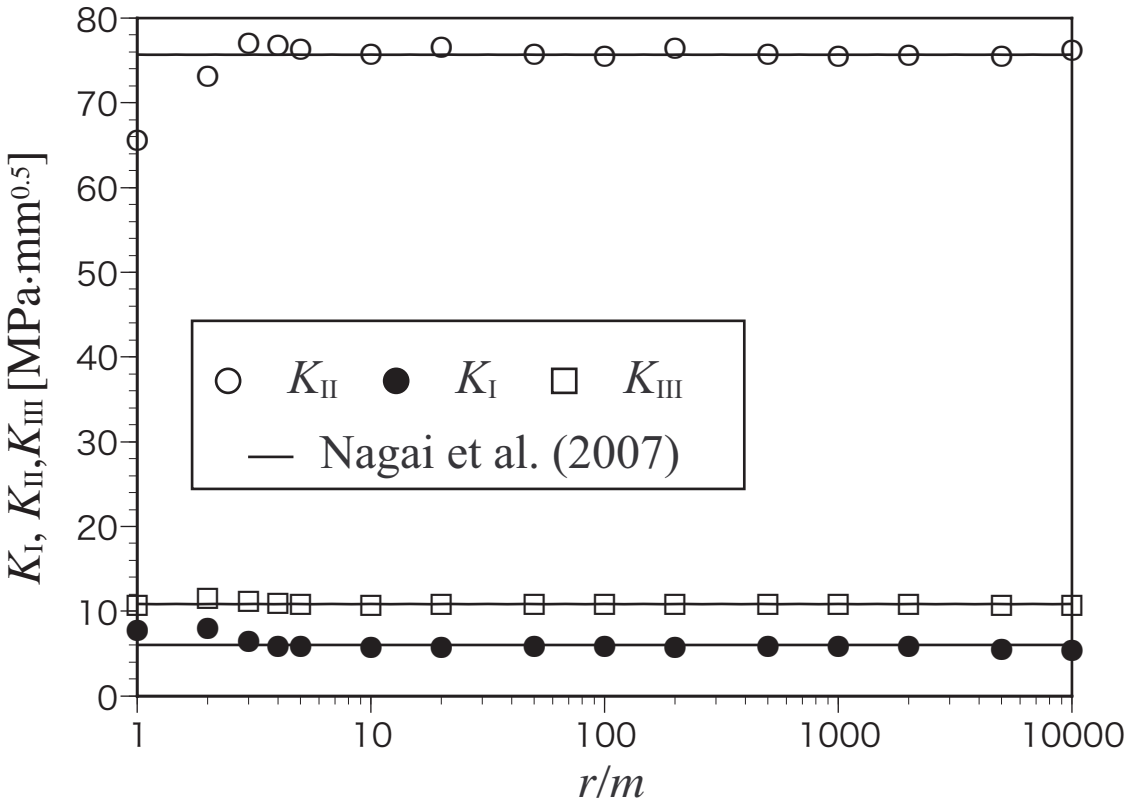

Fig. 15 Stress intensity factors calculated from different H-integral radii.

Table 1 Elastic stiffness C_{ij} (GPa) and CTE. α_{ij} ($10^{-6}\mathrm{K}^{-1}$) of anisotropic materials.

		Silicon (Cubic)	Aragonite (Orthotropic)	GSO (Monoclinic)
Elastic Stiffness	C_{11}	165.7	160	223
	C_{12}	63.9	36.6	108
	C_{13}	63.9	1.97	98.5
	C_{15}	0	0	84
	C_{22}	165.7	87	150
	C_{23}	63.9	15.9	102
	C_{25}	0	0	33.3
	C_{33}	165.7	85	251
	C_{35}	0	0	–6
	C_{44}	79.56	41.3	78.8
	C_{46}	0	0	6.6
	C_{55}	79.56	25.6	68.8
	C_{66}	79.56	42.7	82.7
CTE.	α_{11}	3.5	35.0	4.4
	α_{22}	3.5	17.0	14.0
	α_{33}	3.5	10.0	6.8
	α_{31}	0	0.0	-1.4

Table 2 Calculated stress intensity factors of an interfacial corner between glass-silicon bimaterials ($\alpha = 180^{\circ}, \beta = 125.26^{\circ}$).

r	K_{I}	K_{II}	K_{III}
mm	$\mathrm{MPa}\cdot\mathrm{mm}^{0.497}$ $l_k = 10\mu m$		
0.001	1.447	3.834	0
0.005	1.487	3.858	0
0.01	1.479	3.848	0
0.03	1.490	3.864	0
0.05	1.491	3.860	0
0.08	1.489	3.859	0

Table 3 Calculated eigenvalues, scalar coefficients, and stress intensity factors of an interfacial corner between aragonite-GSO bimaterials ($\alpha = 180^{\circ}, \beta = 160^{\circ}$).

	I	II	III
λ	0.5167+0.042i	0.5167–0.042i	0.5200
C	–0.2254+0.1066i	–0.2254–0.1066i	4.980
K	3.278	22.90	35.09

Unit : $C_k \ldots \mathrm{MPa} \cdot \mathrm{mm}^{1-\lambda_k}$ $K_{\mathrm{I}}, K_{\mathrm{II}}, K_{\mathrm{III}} \ldots$ $\mathrm{MPa} \cdot \mathrm{mm}^{0.483}$ $l_k = 10\mu m$